



HAL
open science

Dynamics and phase decomposition in a cylinder wake

Majd Armaly, Emilien Varea, Corine Lacour, Luminita Danaila, Bertrand Lecordier

► **To cite this version:**

Majd Armaly, Emilien Varea, Corine Lacour, Luminita Danaila, Bertrand Lecordier. Dynamics and phase decomposition in a cylinder wake. 25e Congrès Français de Mécanique,, Aug 2022, Nantes, France. hal-04280025

HAL Id: hal-04280025

<https://hal.science/hal-04280025>

Submitted on 10 Nov 2023

HAL is a multi-disciplinary open access archive for the deposit and dissemination of scientific research documents, whether they are published or not. The documents may come from teaching and research institutions in France or abroad, or from public or private research centers.

L'archive ouverte pluridisciplinaire **HAL**, est destinée au dépôt et à la diffusion de documents scientifiques de niveau recherche, publiés ou non, émanant des établissements d'enseignement et de recherche français ou étrangers, des laboratoires publics ou privés.

Dynamics and phase decomposition in a cylinder wake

Majd Armaly^a Emilien Varea^a

Corine Lacour^a Luminita Danaila^b Bertrand Lecordier^a

a. CORIA UMR 6614, University of Rouen Normandy and INSA Rouen,
majd.armaly@coria.fr

b. M2C UMR 6143, University of Rouen Normandy, luminita.danaila@univ-rouen.fr

Abstract :

The far aim of the study is to assess experimentally the dynamical behavior of a wake behind a cylinder, as a function of the upstream flow. The wake behind the obstacle is composed of coherent motion (CM) and random motion (RM). Coherent motion, reminiscent of the Von Kármán street, interacts with the random flow, thus inducing locally enhanced turbulent cascade. This exchange in energy between CM & RM is reflected by the kinetic energy budget at one point.

A cylinder is placed in closed loop wind tunnel to create Von Kármán vortex street. The Reynolds number, based on the cylinder diameter and the free main stream velocity, is equal to $Re = 2581$. Two-dimensional, two-components in-plane velocity fields are measured behind the cylinder by Particle Image Velocimetry (PIV). Two sets of measurements are explored: without and with synchronization based on the CM. For synchronization, a microphone is used. CM is reconstructed, with 9 phase shifts.

Key words : *Turbulence - Wakes - Triple decomposition - Energy budgets for turbulent kinetic energy*

1 Introduction

Wakes are widely observed on our planet, in both environmental and industrial flows, as a result of the presence of solid bodies in fluids. Flow over bluff bodies have been subject of interest for many years. When a fluid flow passes over an obstacle, staggered vortices are created downstream. This is called Bénard–Von Kármán street, studied by e.g. Bloor (1966) [2], Roshko (1954) [3] and Williamson(1996) [6]. Unal & Rockwell (1988) [5], Abernathy & Kronauer (1961) [8] and Triantafyllou & Chryssostomidis (1986) [9] assessed the formation of the Von-Kármán street in the context of the absolute instabilities of shear layers. At higher Reynolds numbers, turbulent flows behind cylinders exhibit a wide range of scales, with different amounts of energy. The classical postulates of turbulence are based upon the concept of the cascade, i.e. kinetic energy is

injected at the largest scales of the flow and is transferred to smaller scales through the cascade process. Cantwell & Coles (1983) [11] showed that a substantial fraction of the turbulent kinetic energy is primarily produced at intermediate scales near saddle points, and is later transported towards larger scales.

The assessment of the energy budget in the near-wake region of a cylinder allows to detect the basic mechanisms of production, transport and dissipation of kinetic energy. Townsend [4] illustrated the turbulent kinetic energy budget for different shear flows. Instability of the shear layer is associated with production and transport of kinetic energy, whilst in other regions of the flow all processes are present.

The experimental study of Thiesset [10] assessed the turbulent kinetic energy budget in the cylinder wake. Measurements were based on hot wire anemometry, which is time-resolved but focuses on a single space point. Moreover, all phases of vortex shedding are mixed together, and a careful selection of each phase was required in order to discern processes at each specific phase.

The present contribution resolves this shortcoming by the use of high-fidelity optical diagnostics that offers a wider view of the flow. Moreover, measurements are performed at each particular phase of the coherent motion (CM) (any particular time in its period is usually called phase), which further simplifies the analysis. In this contribution, we focus on assessing the dynamical behavior of a wake behind a cylinder as a function of the upstream flow, for a low Reynolds number ($Re \equiv \frac{DU}{\nu} = 2581$). The Strouhal number $St \equiv \frac{fD}{U} = 0.2$, where D is the diameter of the cylinder, ν is the kinematic viscosity, U is the free stream velocity and f is the shedding frequency. The Strouhal number St may depend on different parameters such as the Reynolds number, the geometry of the obstacle, the upstream turbulence level, the cylinder roughness.

Section 2 is devoted to the experimental setup and measurements parameters. The triple decomposition and the statistics are described in Section 3. In Section 4, results pertaining to the turbulent kinetic energy are presented. We conclude in Section 5.

2 Experimental set-up

The experimental study was performed in a closed loop wind tunnel at CORIA laboratory in France. The test section of the wind tunnel is a square section with dimensions of $40 \times 40 \text{ cm}^2$ and 2.5m long. The fan is located after the divergence part of the wind tunnel with a 2 HP power and a max frequency of 60Hz. The cross section is drilled at its end with an 80mm hole to insert the smoking machine tube for particles injection. The walls of the test section allow optical diagnostics to be performed. The tunnel speed is controlled by a frequency controller which modulated fan rotation speed. The velocity of the tunnel ranges from 0.23m/s to 16.6m/s. The free stream is uniform with a residual turbulence intensity smaller than 1%. A cylinder of 1cm diameter is fixed in the tunnel to generate the turbulent wake.

2D-2C PIV measurements were carried out in the test section of the wind tunnel. JAI camera with a resolution of $2048 \times 2048 \text{ pixels}^2$ (12 bits), working at 8 fps were used for

data acquisition. A Nd:YAG laser (532nm) was used to illuminate $10.4 \times 10.4 \text{cm}^2$ field of view. Its maximum frequency is of 10Hz. The laser beam passed through a beam expander, spherical lens ($f=1000 \text{ mm}$), cylindrical lens ($f=-100 \text{ mm}$) and a mirror, see [Figure 1]. The laser sheet at the focus line is 0.5mm thick. Time between pulses was of $20 \mu\text{s}$. The PIV post processing was performed using the in-house code developed by Dr. B. Lecordier. The size of the interrogation window was $32 \times 32 \text{pixels}^2$ ($1.6 \times 1.6 \text{mm}^2$). Overlap was set to 50%, yielding a 127×127 vector field.

Data acquisition was synchronized with the vortex generation, thus allowing to resolve characteristic phases of the coherent motion (CM) and to eventually lead to a visualisation of the of Von Kármán vortex street. Synchronisation of data acquisition with CM generation requires first a clear detection of vortices, and of their dynamics, just behind the cylinder. Vortices detection was performed by placing a microphone sensor (Type: 4182, and sensitivity: 3, 65 mv/Pa), just after the cylinder, to estimate the dynamical pressure of the flow. The sampling rate was set to 20 kHz. The pressure signal obtained from the microphone is quasi-periodic, thus indicating all phases of vortices (or, CM) generation. Data acquisition was performed for particular phases of CM, using trigger systems.

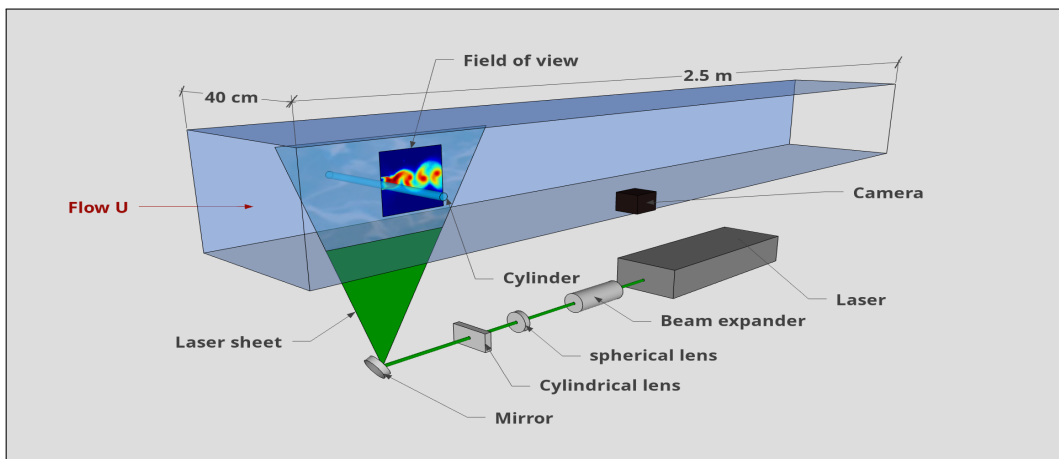


Figure 1: Experimental setup.

Images acquisition was performed with a commercial software (DANTEC). Non-synchronized data were recorded as well, as a baseline case, Table 1. Images were acquired through the phase-conditioning technique described earlier (microphone synchronization) for 9 different phase shifts, Table 2.

Non-synchronized Data				
Re number	St number	shedding freq. (Hz)	Phase shifts	Couple of images
2581	0.2	60	no phase shifts	10000

Table 1: Parameters of non-synchronized data.

Synchronized Data				
Re number	St number	shedding freq. (Hz)	Phase shifts	Couple of im- ages
2581	0.2	60	9 phase shifts each 4ms	5000

Table 2: Parameters of synchronized data.

3 Phases decomposition verification of the wake

3.1 Mean and RMS of the stream-wise velocity

The nearly periodic nature of the flow, due to the Von Kármán vortices, allows for the concept of phase to be defined, and, on the basis of our technique, properly assessed from data. Phase-averaged statistics (i.e., computed for each phase of the CM) may thus be appraised.

The quality of phase decomposition must be first checked on lower-order statistics, such as the mean of the velocity field and Root Mean Squared. Figures 2(a),(d) show the mean velocity and the RMS (Root-Mean-Squared) of the stream-wise velocity component, with no distinction among phases (without microphone synchronization). Figures 2(b),(e) and Figures 2(c),(f) represent the mean velocity and the RMS at $\phi = 0^\circ$ and $\phi = 180^\circ$, respectively (therefore, with microphone synchronization). Figures 2(e),(f) reveal the vortex street in the wake, by figuring out the fluctuations at a particular phase of acquisitions. RMS is maximum in regions where shear is most important and gradually decreases downstream behind the obstacle. The spatial distribution of the Vortex-street patterns at $\phi = 0^\circ$, is typically opposed to that at $\phi = 180^\circ$. This emphasizes the precision of the microphone synchronization in the Particle Images Velocimetry (PIV) measurements system.

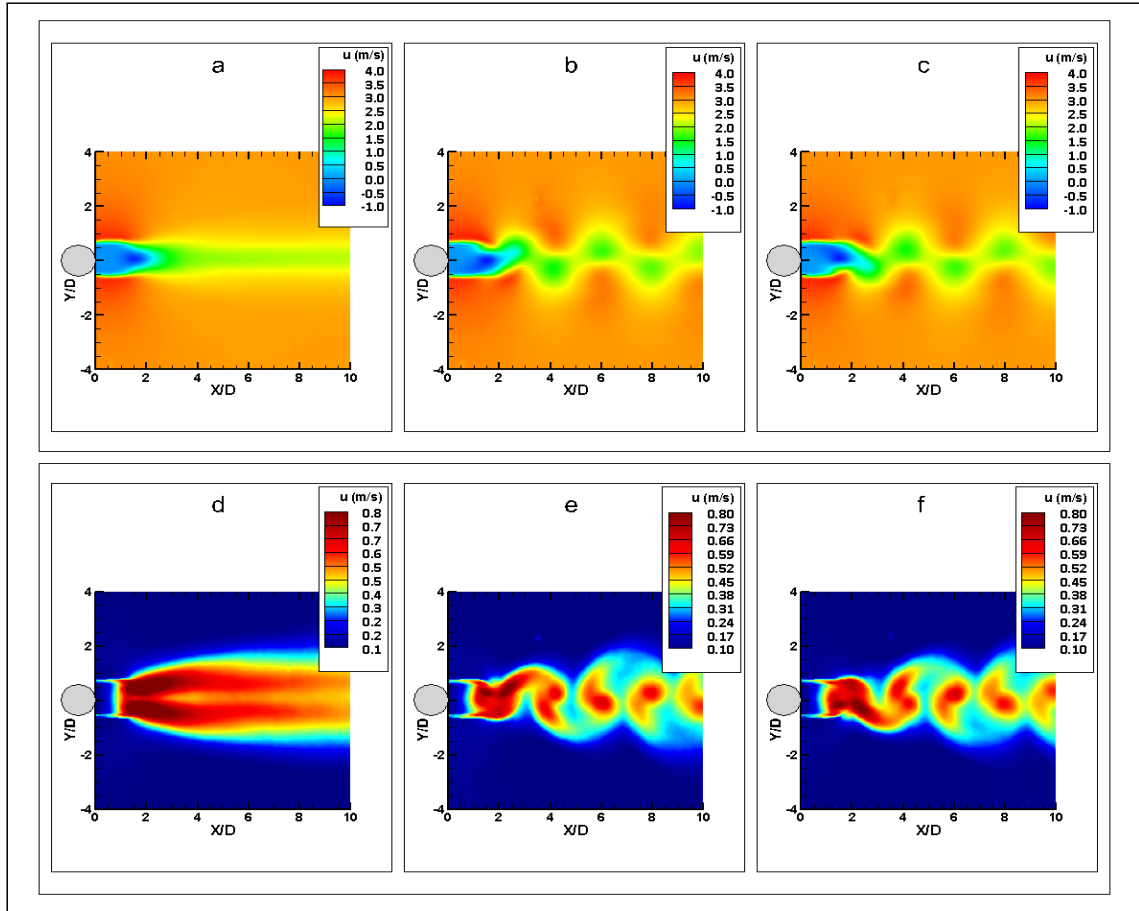


Figure 2: (a) and (d) are the non synchronized mean velocity and RMS along x direction, respectively. (b) and (e) are the synchronized mean velocity and RMS along x direction at $\phi = 0^\circ$, respectively. (c) and (f) are the synchronized mean velocity and RMS along x direction at $\phi = 180^\circ$, respectively.

3.2 Triple decomposition

Triple decomposition is a mathematical decomposition of turbulent fields which accounts for the quasi-periodicity of the CM, for each phase. Tracking the CM and its dynamics provides a significant insight into the nature of the flow.

The first term in (Eq. 2) represents the temporal average of the whole instantaneous field. The second term in (Eq. 2) accounts for the coherent motion (CM) and is quasi-periodicity. The third term in (Eq. 2) delineates the random motion (RM). This equation corresponds to the decomposition first proposed by Hussein and Reynolds [7] for an organized wave, further used as a clock for selecting samples. They decomposed the instantaneous turbulent field $f(x, t)$ into three main components: time average $\overline{f(x, t)}$ (mean of the non-synchronized data), the random fluctuations in an instantaneous field $f_r(x, t)$ and the coherent structures (CM) $f_c(x, t)$, (Eq. 1). Coherent motion (CM) is obtained by difference between the phase average $\langle f(x, t) \rangle$ (mean of the synchronized data) and the time average $\overline{f(x, t)}$, (Eq. 2).

$$\underbrace{f(x, t)}_{\text{Instantaneous}} = \underbrace{\overline{f(x, t)}}_{\text{Time average}} + \underbrace{f_c(x, t)}_{\text{Coherent motion}} + \underbrace{f_r(x, t)}_{\text{Random motion}} \quad (1)$$

$$\underbrace{f_c(x, t)}_{\text{Coherent motion}} = \underbrace{\langle f(x, t) \rangle}_{\text{Phase average}} - \underbrace{\overline{f(x, t)}}_{\text{Time average}} \quad (2)$$

The random fluctuations are found by difference between the instantaneous velocity field and the phase average, (Eq. 3),

$$\underbrace{f_r(x, t)}_{\text{Random motion}} = \underbrace{f(x, t)}_{\text{Instantaneous}} - \underbrace{\langle f(x, t) \rangle}_{\text{Phase average}} \quad (3)$$

Figure 3 shows the instantaneous triple decomposition of the wake, at $Re = 2581$ and at phase $= 0^\circ$. Function $f(x, t)$ is the summation of the three components that is equal to the instantaneous velocity field, Eq. 1. To check the validity of this decomposition, the instantaneous velocity field should be equal to the sum of the three components.

Coherent motion is dominant near the cylinder, but gradually weakens before disappearing as the distance from the cylinder increases, as shown in $f_c(x, t)$ of Figure 3. Coherent motion (CM) renders the flow more complex, as it induces additional shear and interactions with other scales of the motion. Coherent motion enhances the exchange of energy between different flow components. One way to detect and assess energy production and exchange mechanisms is to investigate the turbulent kinetic energy (TKE) budget. TKE budget evidences how Coherent motion contributes to different phenomena.

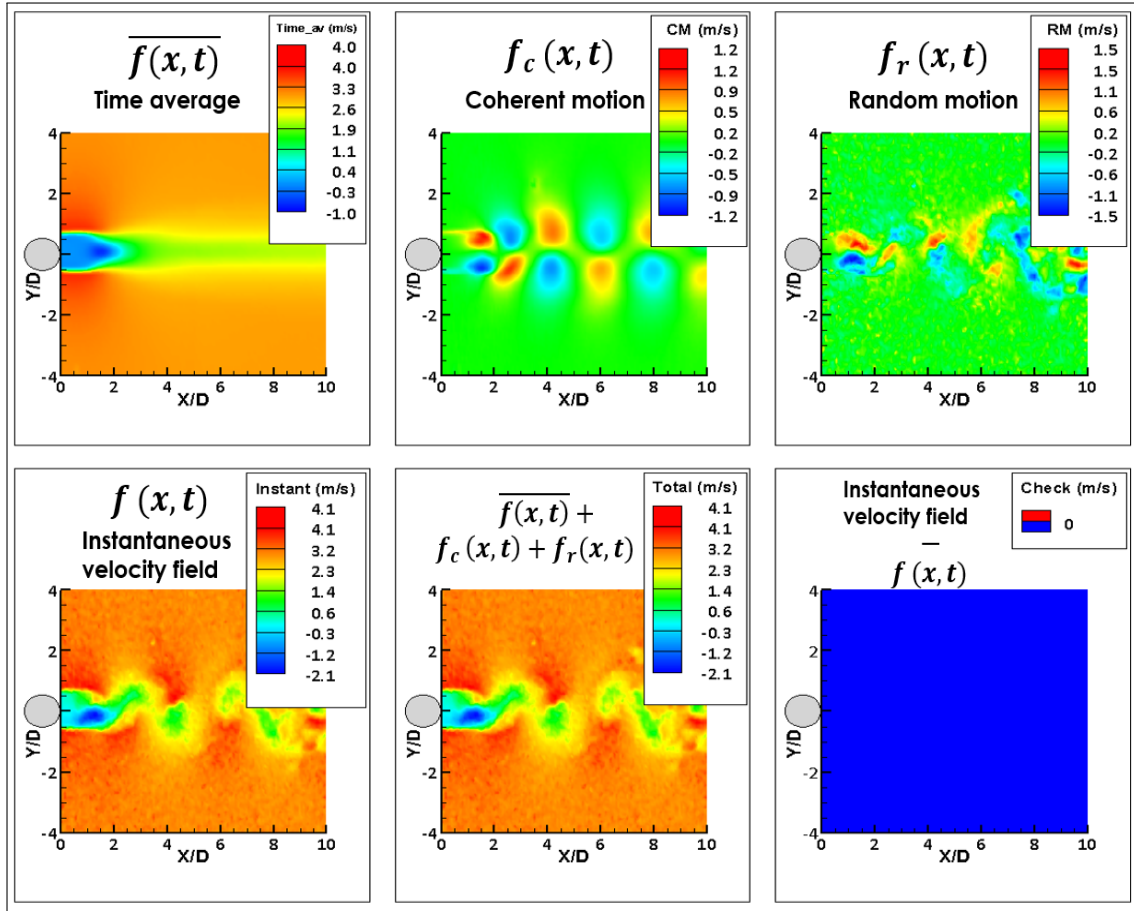


Figure 3: Triple decomposition for $Re = 2581$ and $\phi = 0^\circ$.

4 Turbulent kinetic energy

We made sure that all phases of the CM are correctly extracted through the technique based on the microphone reference. Transport equation for the turbulent kinetic energy is further reported. This equation explains the nature and the mechanics of the turbulence in the flow at one point, (Eq. 4).

$$\underbrace{\left(U \frac{\partial(\overline{0.5q^2})}{\partial x} + V \frac{\partial(\overline{0.5q^2})}{\partial y} \right)}_{\text{Advection}} + \underbrace{\left(\overline{uv} \frac{\partial U}{\partial y} \right)}_{\text{Generation}} + \underbrace{\left(\frac{\partial \overline{pv}}{\partial y} + \frac{\partial(\overline{0.5q^2 v})}{\partial y} \right)}_{\text{Diffusion}} + \underbrace{\epsilon}_{\text{Dissipation}} = 0 \quad (4)$$

In this equation Eq. (4), U and V are the mean velocities along x and y directions respectively. Terms u and v represent the fluctuations of the instantaneous velocity field along x and y direction respectively. q^2 represents the kinetic energy, computed with the axisymmetry hypothesis ($2u^2 + v^2$) [10]. Finally, ϵ is the kinetic energy dissipation rate. The TKE transport equation contains 4 main terms (Advection, Generation, Diffu-

sion and Dissipation). The first term in the equation is the advection, or the transport of the fluctuations due to mean velocity. Advection terms along x and y directions are reported. Generation of turbulent energy is the second term, and will be greatest near the position of maximum shear and zero along the axis of symmetry. It represents the exchange of kinetic energy between the mean flow and turbulent fluctuations. In general, the energy exchange involves a loss of the mean flow and gain to the turbulence. The third term is the diffusion, which is divided into diffusion due to pressure and diffusion due to turbulence. Turbulent diffusion term explains how the turbulent kinetic energy is diffused from locations where it is produced, to other places where production is smaller, or absent. The last term is the dissipation (occurring at smallest scales, or Kolmogorov scales), and reflects the work done by smallest eddies against viscous stresses. As our analysis is based upon 2D-2C PIV, terms involving derivatives are not available. For instance, it is well known that the energy dissipation rate is underestimated. Other methods are to be used to assess the correct values of this quantity. The dissipation rate ϵ_{PIV} is first computed by Eq. (5), and then corrected using J. G. Chen & T.M Zhou (2018) [12] data to get access to the non-resolved data. The dissipation rate ϵ_{PIV} (computed from PIV data) is much smaller than the values of ϵ estimated with hot wire anemometry [12]. Therefore, a correction is applied to ϵ_{PIV} to reach the values reported by [12] for the same flow, and for the same Reynolds number.

$$\epsilon_{PIV} = \gamma \left[\frac{5}{3} \overline{\left(\frac{\partial u}{\partial x}\right)^2} + 2 \overline{\left(\frac{\partial u}{\partial y}\right)^2} + \overline{\left(\frac{\partial v}{\partial x}\right)^2} + \frac{8}{3} \overline{\left(\frac{\partial v}{\partial y}\right)^2} \right]. \quad (5)$$

4.1 Non-synchronized data

Figure 4 shows all terms in Eq. (4), for non-synchronized data. All terms appear to be important for the first few diameters downstream, and are symmetric with respect to the center line of the wake. The terms exhibit zero values in a region just behind the cylinder, that represents the recirculation zone. Pressure field is not available experimentally, therefore the pressure-diffusion term cannot be estimated. Therefore, this term is calculated with the TKE equation, by difference. Diffusion through pressure is thus determined from the budget equation, by considering that all the other terms are correctly evaluated. Figures 4 (a),(b) show the advection along x and y directions, respectively. These terms indicate the transport of the fluctuations by the mean flow. Figures 4 (d),(e) depict the diffusion through turbulence and through pressure, respectively, which in turn indicate the transport of the fluctuations through turbulence and pressure. The two main terms, advection and diffusion appear to be complementary. The positive regions in advection terms, become negative in diffusion terms and *vice versa*. This shows the conversion from the transport of the kinetic energy of the mean velocity to the transport of the kinetic energy by the fluctuation quantities. Figure 4 (c) shows the generation term map, revealing that the maximum takes place where the maximum gradient of the mean velocity and the maximum level of anisotropy ($\overline{u^2}/\overline{v^2} > 1$ or $\overline{u^2}/\overline{v^2} < 1$) occur. Figure 4 (f) shows the dissipation term, it shows the

maximum at the center line of the wake. The dissipation is maximum where higher strain and shear occur, which enhances the energy of the small scales. All terms show a good agreement with the results obtained by F. Thiesset [10].

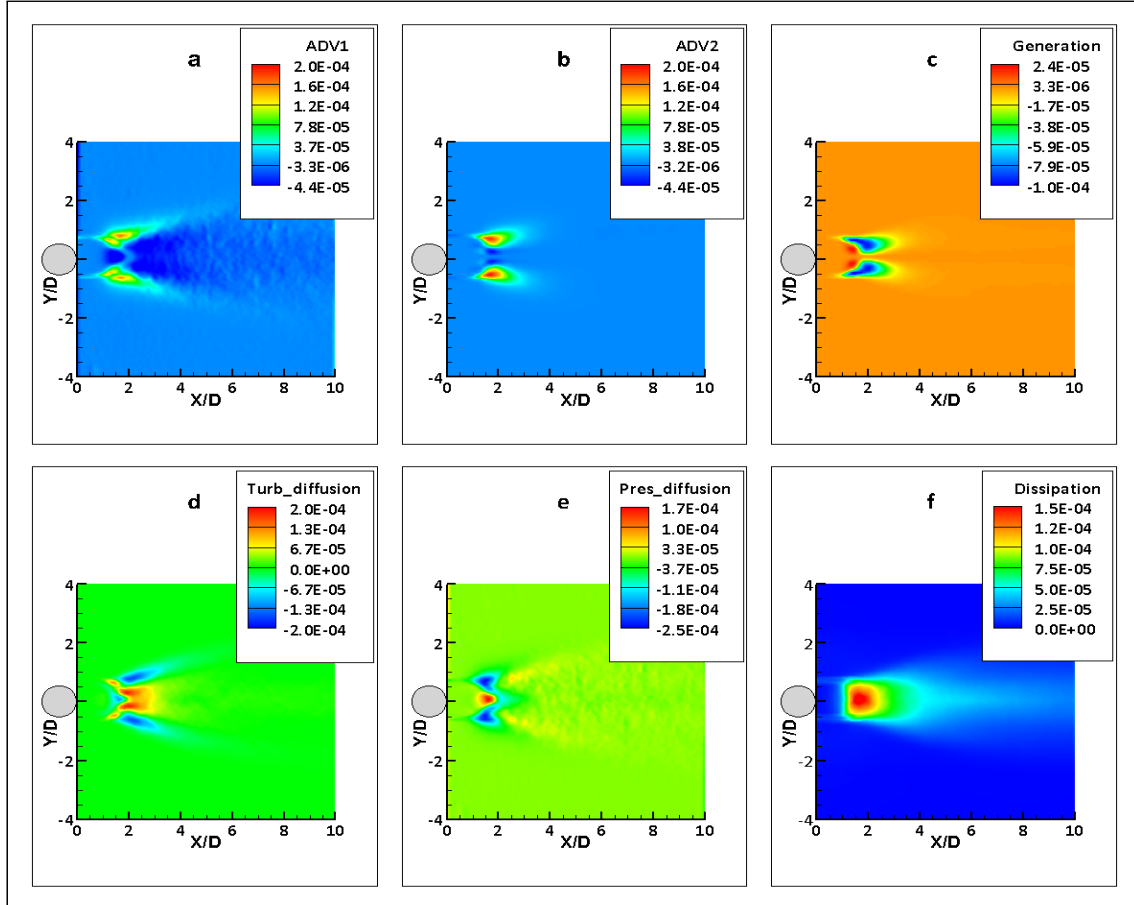


Figure 4: One-point turbulent kinetic energy balance at $Re = 2581$ without microphone synchronization. All the terms are normalised by D/U_0^3 . (a) Advection on x direction term $U \frac{\partial(0.5\overline{q^2})}{\partial x}$. (b) Advection on y direction term $V \frac{\partial(0.5\overline{q^2})}{\partial y}$. (c) Generation term $\overline{uv} \frac{\partial U}{\partial y}$. (d) Diffusion term through turbulence $\frac{\partial 0.5\overline{q^2 v}}{\partial y}$. (e) Diffusion term through pressure $\frac{\partial \overline{pv}}{\partial y}$. (f) Dissipation term ϵ

Figure 5 shows profiles parallel to y direction at $X/D = 2$, starting from the center line of the wake. Total advection and total diffusion have the same trace with different signs as discussed before. The dissipation is maximum at the center line of the cylinder and gradually decreases. The generation is zero at the center line and maximum in high shear regions. This is in agreement with the previous studies of Townsend [4] performed at higher Reynolds number (8400) and using hot wire anemometry.

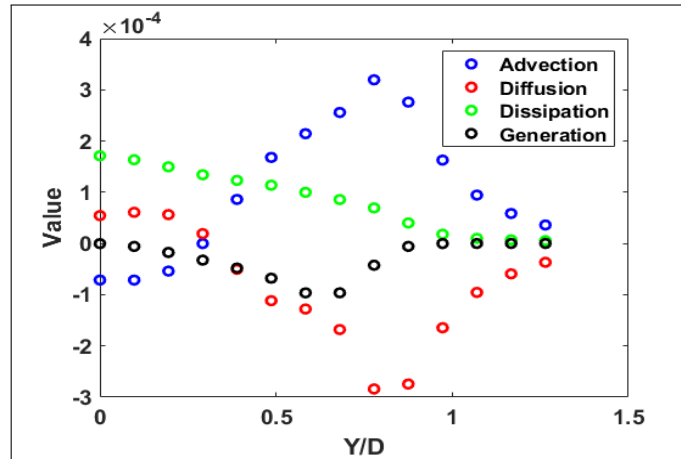


Figure 5: TKE terms profiles for non synchronized data, at Reynolds no.=2581 ($X/D = 2$).

4.2 Synchronized data

The validation of the data non-synchronized through literature, allows us to move forward with the TKE computation of the data synchronized with the microphone. Figures 6a,6b show advection along x and y directions, respectively, for synchronized data and for 4 different phases. This shows the evolution of the transport by the mean flow between the phases. Figure 6a shows at each vortex of the Von-Kármán street, positive and negative advection values follow each other, yielding to a source of vorticity. Figure 6b shows high advection just behind the cylinder where the rolling-up process starts.

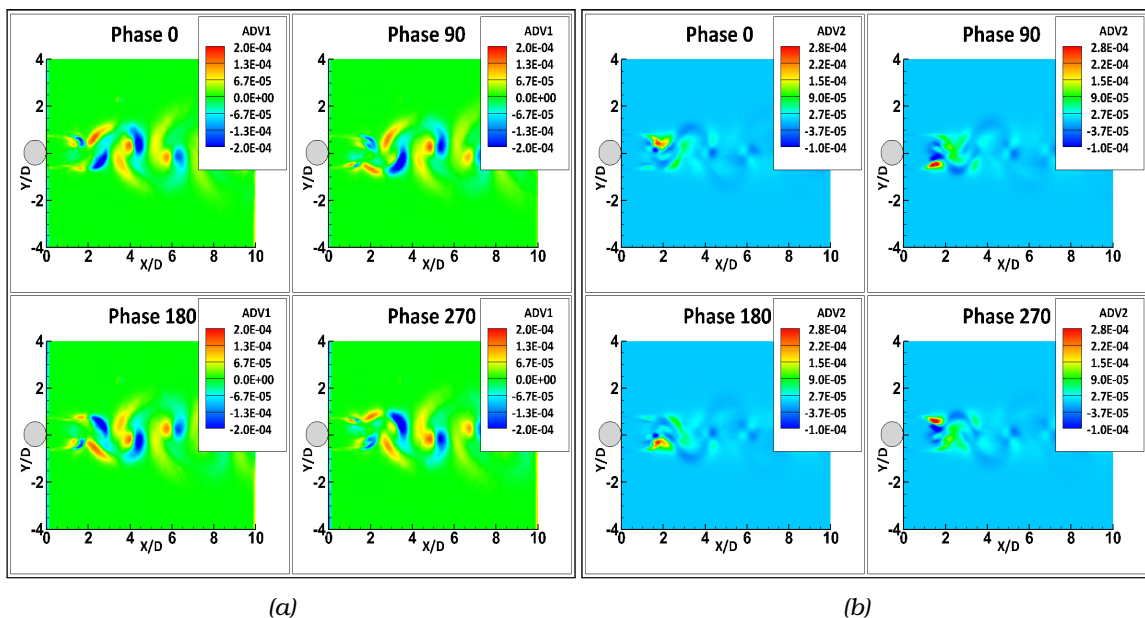


Figure 6: One point turbulent kinetic energy balance at $Re = 2581$ with microphone synchronization at $0^\circ, 90^\circ, 180^\circ$ and 270° phase shifts. All the terms are normalised by D/U_0^3 . (a) Advection on x direction term $U \frac{\partial(0.5q^2)}{\partial x}$. (b) Advection on y direction term $V \frac{\partial(0.5q^2)}{\partial y}$.

Figures 7a,7b show diffusion through turbulence and diffusion through pressure for different phases, respectively. As aforesaid, the kinetic energy is carried from generation regions, through the advection and diffusion processes. This is shown at $(X/D = 2, Y/D = 0.5)$ at any phase, for instance.

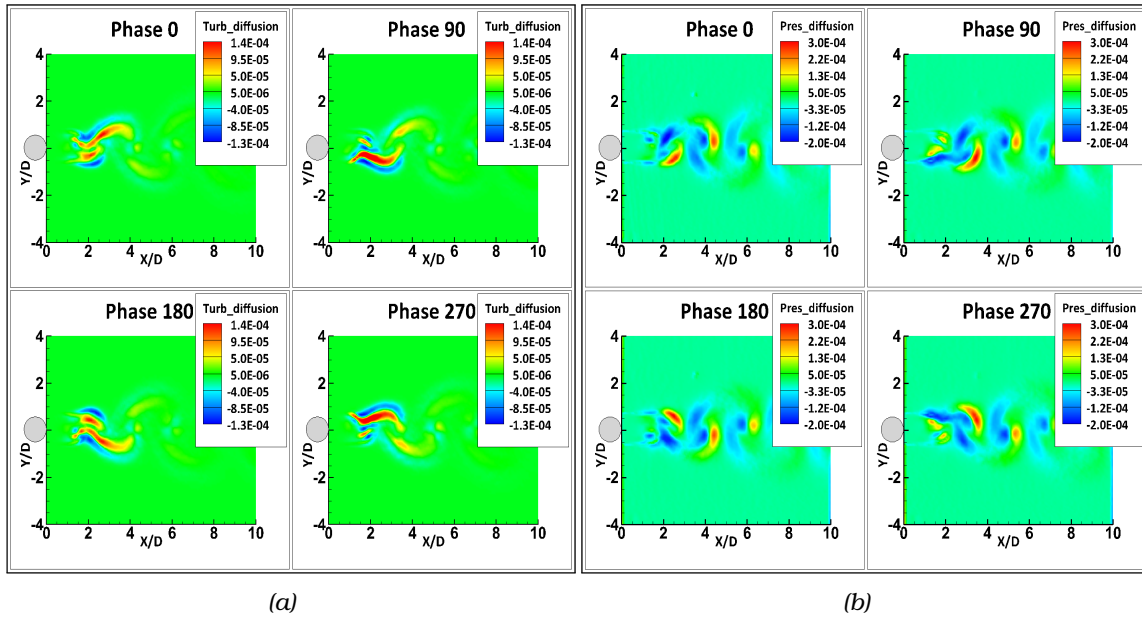


Figure 7: One-point turbulent kinetic energy balance at $Re = 2581$ with microphone synchronization at $0^\circ, 90^\circ, 180^\circ$ and 270° phase shifts. All terms are normalised by D/U_0^3 . (a) Diffusion through turbulence $\frac{\partial(0.5q^2v)}{\partial y}$. (b) Diffusion through pressure $\frac{\partial \overline{pv}}{\partial y}$.

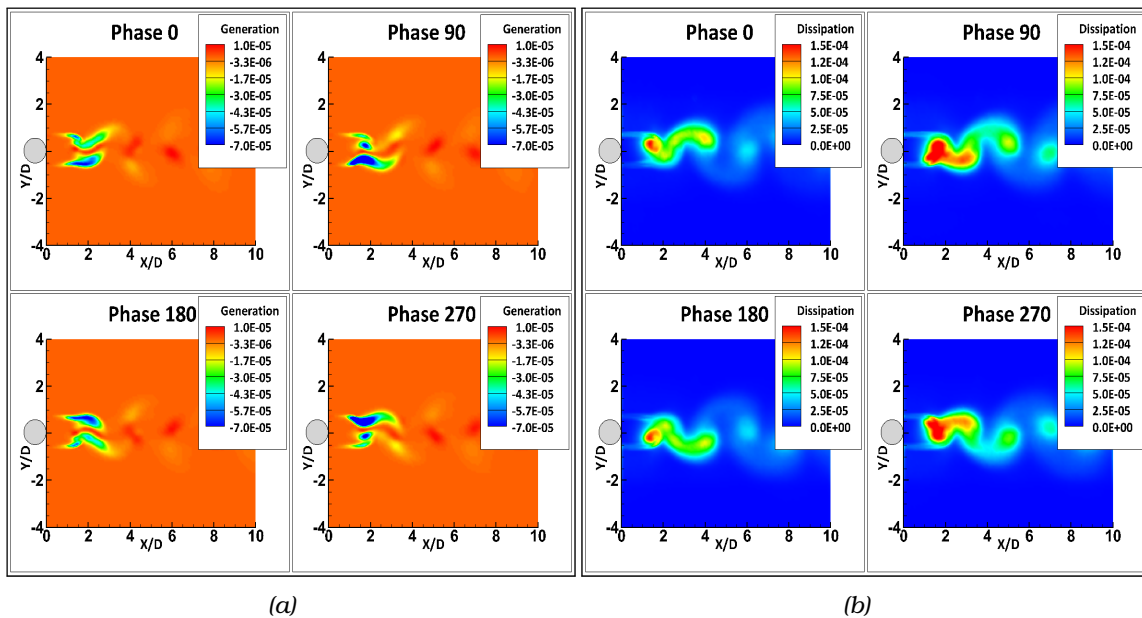


Figure 8: One-point turbulent kinetic energy balance at $Re = 2581$, with microphone synchronization at $0^\circ, 90^\circ, 180^\circ$ and 270° phase shifts. All terms are normalised by D/U_0^3 . (a) Generation term $\overline{wv} \frac{\partial U}{\partial y}$. (b) Energy dissipation rate term ϵ .

Figures 8a,8b show the generation and the dissipation terms for different phases, respectively. Figure 8a shows the vortices generation, which is associated to the onset of the Von-Kármán street. The dissipation rate is distributed over the whole flow and is not necessarily large in regions of strong generation, as shown in Figure 8b. However, the maximum dissipation is very close to the cylinder, and this increases at phase 90° and phase 270° . As previously shown in synchronized data, all terms change sign after a half period. This shows the accuracy of the phase decomposition in the wake.

5 Conclusion

The present study is an analysis of the cylinder wake dynamics as a function of the upstream flow. Microphone sensor is installed in the flow to synchronize the data acquisition to coherent structure generation. This technique helps us to assess experimentally phase averages, with high resolution and without resorting to numerical methods. Validation of the phase decomposition is done through the computation of turbulence statistics (mean and RMS) and through the triple decomposition method. TKE (Turbulent kinetic energy) assessment was carried out for both non-synchronized and data synchronized with microphone. TKE computations were performed for different phases to get an insight into the energy exchanges and their evolution at different phases or the flow. The distributions of different terms as a function of the phase change sign after a half period, which guarantees the correct phase decomposition of the motion in the wake. Coherent motion (CM) shows its prominence by contributing in wakes TKE exchange.

Acknowledgement

The project (DYNEOL) was funded by the French National Research Agency (ANR) under contract no. ANR-17-CE06-0020

References

- [1] F. Thiesset, L. Danaila and R.A. Antonia, Dynamical interactions between the coherent motion and small scales in a cylinder wake, *Journal of Fluid Mechanics*, 749 (2014) 201–226.
- [2] M. Susan Bloor and J.H. Gerrard, Measurements on turbulent vortices in a cylinder wake, *Journal of Fluid Mechanics*, 1966.
- [3] A. Roshko, On the development of turbulent wakes from vortex street, National Advisory committee for aeronautics, 1954.
- [4] A.A. Townsend, The structure of turbulent shear flow, University of Cambridge, The pitt building, trumpington street Cambridge CB2 1RP, 1976.

- [5] M.F. Unal and D. Rockwell, On vortex formation from a cylinder. part 1. the initial instability, *Journal of Fluid Mechanics*, 190, 1988.
- [6] C. Williamson, Vortex dynamics in the cylinder wake, *Journal of Fluid mechanics*, 28, 1996.
- [7] A.K.M.F. Hussain and W.C. Reynolds, The mechanics of an organized wave in turbulent shear flow, *Journal of Fluid Mechanics*, 41-part 2, 1970.
- [8] Abernathy and Krounauer, The formation of vortex streets, *Journal of Fluid Mechanics*, 1961.
- [9] Triantafyllou and Chryssostomidis, On the formation of vortex streets behind stationary cylinders, *Journal of Fluid Mechanics*, Volume 170, 461-477, 1986.
- [10] F. Thiesset, Exploration analytique et expérimentale des interactions cohérence-turbulence au sein d'un écoulement de sillage, Université de Rouen, 2011, HAL Id : tel-00880987 <https://tel.archivesouvertes.fr/tel-00880987>.
- [11] B. Cantwell and D. Coles, An experimental study of entrainment and transport in the turbulent near wake of a circular cylinder, *Journal of Fluid Mechanics*, Volume 136, 321-374, 1983.
- [12] J.G. Chen and T.M. Zhou, Characteristics of the turbulent energy dissipation rate in a cylinder wake, *Journal of Fluid Mechanics*, Volume 835, 271-300, 2018.